THE JOURNAL OF PHYSICAL CHEMISTRY C

Article

pubs.acs.org/JPCC

Transient Excited-State Absorption and Gain Spectroscopy of a Two-Photon Absorbing Probe with Efficient Superfluorescent Properties

Kevin D. Belfield,*[,†,‡] Mykhailo V. Bondar,[§] Alma R. Morales,[†] Xiling Yue,[†] Gheorghe Luchita,[†] and Olga V. Przhonska[§]

[†]Department of Chemistry and [‡]CREOL, The College of Optics and Photonics, University of Central Florida, P.O. Box 162366, Orlando, Florida 32816-2366, United States

[§]Institute of Physics, Prospect Nauki, 46, Kiev-28, 03028, Ukraine

Supporting Information

ABSTRACT: The synthesis, linear photophysical properties, two-photon absorption (2PA), excited-state transient absorption, and gain spectroscopy of a new fluorene derivative *tert*-butyl 4,4′-(4,4′ (1*E*,1′*E*)-2,2′-(9,9-bis(2-(2-ethoxyethoxy)-ethyl)-9H-fluorene-2,7-diyl)bis(ethene-2,1-diyl)bis(4,1 phenylene)]dipiperazine-1-carboxylate (**1**) are reported. The steady-state linear absorption and fluorescence spectra along with excitation anisotropy, fluorescence lifetimes, and photochemical stability of **1** were investigated in a number of organic solvents at room temperature. The 2PA spectra of **1** with a maximum cross section of ∼300 GM were obtained with a 1-kHz femtosecond laser system using open-aperture Z-scan and two-photon-induced fluorescence methods. The transient excited-state absorption (ESA) and gain kinetics of **1** were investigated by a femtosecond pump−probe methodology. Fast relaxation processes (∼1−2 ps) in the gain and ESA spectra of **1** were revealed in ACN solution, attributable to symmetry-breaking effects in the first excited state. Efficient superfluorescence properties of **1** were observed in a nonpolar solvent under femtosecond excitation. One- and two-photon fluorescence microscopy imaging of HCT 116 cells incubated with probe **1** was accomplished, suggesting the potential of this new probe in two-photon fluorescence microscopy bioimaging.

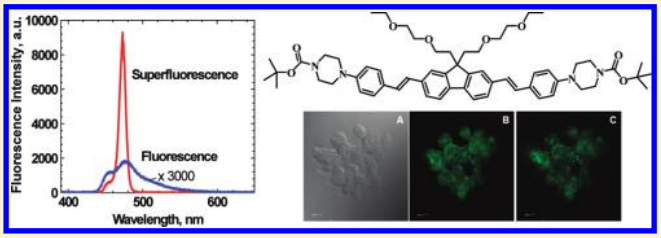

1. INTRODUCTION

Two-photon absorbing organic molecules with specific electronic structures play an important role in a wide variety of nonlinear optical applications, including two-photon laser scanning fluorescence microscopy and biological labeling,[1−3] 3D microfabrication and optical data storage,[4−6] two-photon photodynamic therapy,[7,8] stimulated emission depletion[9,10] upconverted lasing,[11,12] etc. The investigation of the nature of several dynamic processes in organic molecules including transient excited-state absorption (ESA),[13,14] ultrafast vibrational and vibronic relaxations,[15,16] time-resolved fluorescence,[17,18] and transient gain phenomena[19,20] is a subject of great interest for many nonlinear optical applications. The ultrafast photophysics of mono- and dual-branched two-photon absorbing triarylamines was investigated,[21] and a picosecond intramolecular charge transfer bridged by the central triphenylamine was shown. The correlation between excited-state dynamic properties and enhanced two-photon absorption (2PA) efficiency of multibranched chromophores was reported,[22] and the nature of a strong coupling of the Franck−Condon and intramolecular charge transfer states for molecules with increased branching was discussed. Femtosecond transient ESA processes also have been investigated in a number of organic structures, such as β-carotene,[13] photoactive yellow protein (PYP),[14] dimethylamino-substituted diphenylmethane dyes,[23] fucoxanthin,[16] *trans*-4-dicyanomethylene-2-methyl-6-*p*-dimethylamin-ostyryl-4Hpyran,[20] etc., to reveal the nature of excited-state relaxation mechanisms,[16,19] intermediate stages in photochemical reactions,[24] and ultrafast photoinduced energy and charge transfer processes,[16,25] including the role of transient excited electronic states with efficient stimulated emission (gain) properties.[14,23,26,27]

In this paper, fast excited-state relaxation processes along with the linear photophysical and nonlinear optical properties of a new fluorene derivative *tert*-butyl 4,4′-(4,4′ (1*E*,1′*E*)-2,2′-(9,9-bis(2-(2-ethoxyethoxy)ethyl)-9H-fluorene-2,7-diyl)bis-(ethene-2,1-diyl)bis(4,1phenylene)]dipi-perazine-1-carboxylate (**1**) were investigated. The transient ESA, 2PA, superfluorescence, and gain spectroscopic parameters of **1** were obtained with a 1-kHz tunable femtosecond laser system by the corresponding experimental techniques, including open-aperture Z-scan,[28] two-photon-induced fluorescence (2PF),[29] and femtosecond pump−probe[20,24] methodologies. The nature of the electronic structure of **1** was also investigated by semiempirical quantum chemical calculations using HyperChem V7.0 for Windows, and a good agreement between the calculated and experimental data was shown. The high values of the fluorescence quantum yields, efficient 2PA, and super-

Received: March 8, 2012
Revised: April 27, 2012
Published: May 14, 2012

Scheme 1

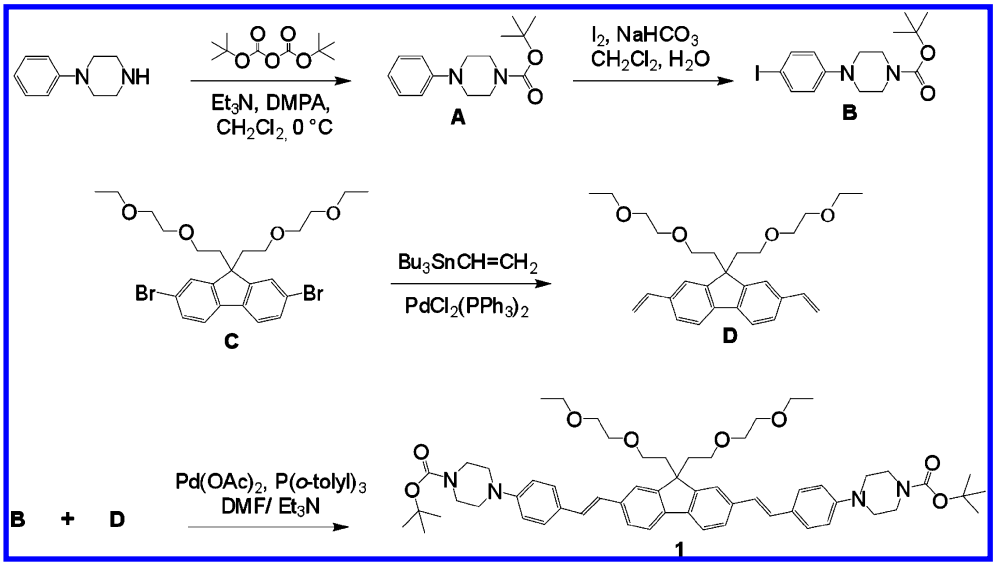

fluorescence properties suggest the potential of **1** for use in a number of important applications, including two-photon-induced fluorescence microscopy (2PFM) techniques.[1,30−32] To demonstrate the potential of probe **1**, one - and two-photon fluorescence microscopy was performed with HCT 116 cells.

2. EXPERIMENTAL SECTION

2.1. Synthetic Procedures. Probe **1** comprises a fluorenyl π-electron bridge with a symmetrical D-π-D chemical structure (where D is an electron donor moiety). Thus, the *N*-phenylpiperazine moiety was used as an electron-donor group (Scheme 1). The synthesis of compound **1** was achieved via the Heck coupling reaction. The synthesis of compound **1** begins with the protection of *N*-phenylpiperazine[1] using di-*tert*-butyl dicarbonate in dichloromethane, providing intermediate **A** in 95% yield. The halogenation of **A**[33] with iodine in a biphasic mixture of aqueous sodium bicarbonate and dichloromethane at room temperature provided intermediate **B** in 80% yield. Pd-catalyzed Stille coupling was performed between dibromofluorene **C** and tributyl(vinyl)tin in refluxing THF in a high-pressure Schlenk tube with $Pd(dppf)Cl_2.CH_2Cl_2$ and CuI. Precursor **D** was obtained in 69% isolated yield. Intermediate **B** was coupled with the aid of the Pd-catalyzed Heck coupling reaction to the divinylfluorene intermediate **C**. The reaction was conducted in a high-pressure Schlenk tube with $Pd(OAc)_2$, tri-*o*-tolylphosphine, and Et_3N as the base in DMF, producing the desired product (**1**) in 52% yield. All compounds were characterized by ^1H NMR, ^{13}C NMR, and high-resolution mass spectroscopy.

*2,7-Dibromo-9,9-bis(2-(2-ethoxyethoxy)ethyl)-9H-fluorene (**C**).* This was prepared according to literature methods.[34] All other reagents and solvents were used as received from commercial suppliers. Melting points were uncorrected. The ^1H NMR and ^{13}C NMR spectra were recorded at 500 and 125 MHz, respectively.

*Synthesis of tert-Butyl 4-phenylpiperazine-1-carboxylate (**A**).* Di-*tert*-butyl dicarbonate (11.5 g, 50.95 mmol) was added in small portions over 15 min to a mixture of *N*-phenylpiperazine (7.66 g, 47.21 mmol), triethylamine (20 mL, 143.68 mmol), and 4-dimethylaminopyridine (DMAP; 0.20 g) in anhydrous CH_2Cl_2 (260 mL) at 0 °C. Ten minutes after the addition was complete, the mixture was warmed to room temperature. After 2 h, the reaction mixture was diluted in water and extracted with CH_2Cl_2. The combined organic extracts were washed with saturated aqueous NaCl, dried over Na_2SO_4, and concentrated to yield 12.0 g (95%, mp = 69−70 °C) of **A**. ^1H NMR (500 MHz, $CDCl_3$) δ: 7.26 (m, 2H), 6.91 (m, 3H), 3.56 (t, J = 4.5 Hz, 4H), 3.10 (t, J = 4.5 Hz, 4H), 1.48 (9H). ^{13}C NMR (125 MHz, $CDCl_3$) δ: 154.7, 151.3, 129.3, 129.0, 120.2, 116.7, 79.8, 49.4, 49.3, 28.5, 28.4, 28.3.

*Synthesis of tert-Butyl 4-(4-iodophenyl)piperazine-1-carboxylate (**B**).* Iodine (11.2 g, 44.2 mmol) was added over 45 min to a mixture of **A** (12 g, 45.77 mmol) and $NaHCO_3$ (5.8 g, 69.0 mmol) in CH_2Cl_2 (175 mL) and water (135 mL), which was kept between 12 and 15 °C. After the addition was complete, the mixture was warmed to room temperature, and the temperature was maintained for 30 min. The mixture was then diluted with CH_2Cl_2 (500 mL) and water (250 mL), and the organic phase was collected and washed consecutively with water (350 mL), a solution of sodium thiosulfate (250 mL), water (3 × 250 mL), and a saturated solution of aqueous NaCl (250 mL). The crude product was dried over Na_2SO_4, concentrated, and recrystallized from *n*-hexane/THF (10/1) to yield 14.2 g (80%, mp =149−150 °C) of **B**. ^1H NMR (500 MHz, $CDCl_3$) δ: 7.52 (d, J = 9 Hz, 2H), 7.52 (d, J = 8.5 Hz, 2H), 3.55 (s, 4H), 3.09 (s, 4H), 1.47 (s, 9H). ^{13}C NMR (125 MHz, $CDCl_3$) δ: 154.6, 150.8, 137.9, 137.7, 118.5, 82.0, 79.9, 48.9, 48.8, 28.5, 28.3, 28.2 ppm.

*Synthesis of 9,9-Bis(2-(2-ethoxyethoxy)ethyl)-2,7-divinyl-9H-fluorene (**D**).* A Schlenk tube was charged with a mixture of 2,7-dibromo-9,9-bis(2-(2-ethoxyethoxy)ethyl)-9H-fluorene (1 g, 1.79 mmol), tributyl(vinyl)tin (3.93 g, 12.39 mmol), $PdCl_2(PPh_3)_2$ (0.05 g, 0.106 mmol), and a few crystals of 2,6-di-*tert*-butylphenol (inhibitor) and 15 mL of toluene at room temperature under N_2. The reaction mixture was degassed for 15 min with N_2. The reaction mixture was heated at reflux for 36 h. Upon completion, the dark brown mixture was diluted with ether and treated with 10% KF aqueous solution. The mixture was stirred for 22 h and followed by vacuum filtration to remove the insoluble solid. The organic mixture was dried over $NaSO_4$ and concentrated. Purification was accomplished by column chromatography using hexane/

dx.doi.org/10.1021/jp302274v | J. Phys. Chem. C 2012, 116, 11261−11271

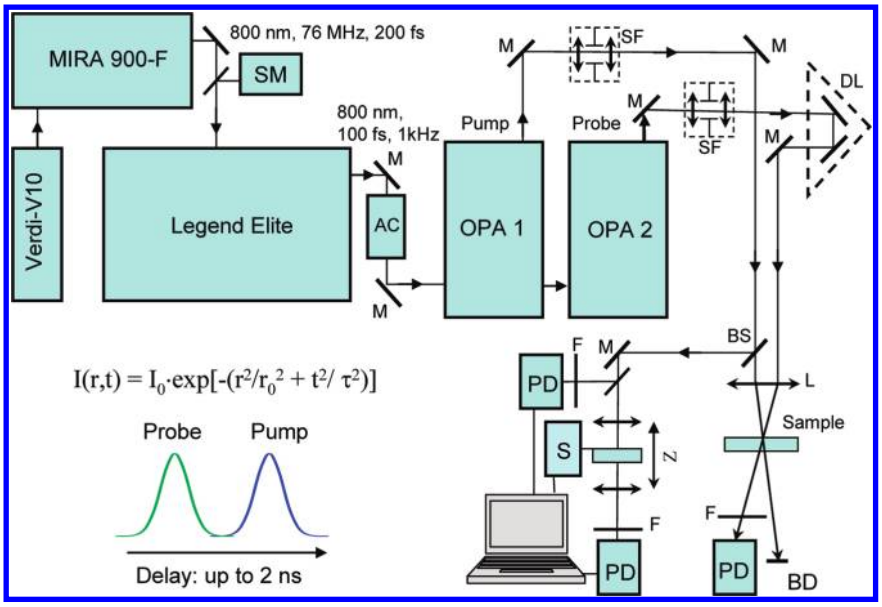

Figure 1. Schematic diagram of the experimental setup: AC, optical autocorrelator; SM, spectrometer; SF, space filters; BS, beam splitter; M, 100% reflection mirrors; DL, optical delay line; PD, calibrated Si photodetectors; L, focusing lenses; F, set of neutral and/or interferometric filters; Sample, 1 mm path length flow cell with sample solution; Z, z-scan setup; S, step motor; BD, beam dump. All laser systems from Coherent, Inc. See text for details.

ethyl acetate (3:2) as an eluent to afford 0.55 g of colorless oil (69% yield). ^{1}H NMR (500 MHz, $CDCl_3$) δ: 7.60 (d, J = 7.5 Hz, 2H), 7.45 (s, 2H), 7.39 (dd, 2H), 6.80 (q, J = 10.5 Hz, 2H), 5.82 (d, J = 10.5 Hz, 2H), 5.29 (d, J = 10.5 Hz, 2H), 3.42 (q, J = 7 Hz, 4H), 3.34 (m, 4H), 3.20 (m, 4H), 2.78 (t, J = 7.5 Hz, 4H), 2.43 (t, J = 7.5 Hz, 4H), 1.14 (t, J = 7.5 Hz, 6H). ^{13}C NMR (125 MHz, $CDCl_3$) δ: 149.50, 139.96, 137.0, 136.8, 125.8, 125.8, 120.7, 120.7, 119.8, 113.5, 113.5, 70.0, 69.6, 67.0, 66.5, 50.9, 39.7, 15.0 ppm. HRMS (ESI-TOF) for $C_{29}H_{38}O_4$ theoretical m/z $[M + H]^+$ = 451.2849; found $[M + H]^+$ = 451.2846.

*Synthesis of tert-Butyl 4,4′-(4,4′-(1E,1′E)-2,2′-(9,9-bis(2-(2-ethoxyethoxy)ethyl)-9H-fluorene-2,7-diyl)bis(ethene-2,1-diyl)bis(4,1-phenylene)]dipiperazine-1-carboxylate (**1**).* *tert*-Butyl 4-(4-iodophenyl)piperazine-1-carboxylate (0.95 g, 2.4 mmol), 9,9-bis(2-(2-ethoxyethoxy)ethyl)-2,7-divinyl-9H-fluorene (0.5 g, 1.11 mmol), $Pd(OAc)_2$ (0.12 g, 0.53 mmol), and P(*o*-tolyl)$_3$ (0.28 g, 0.91 mmol) were transferred to a high-pressure Schlenk tube. To this, 15 mL of a mixture of DMF/Et_3N (5:1) was added. The Schlenk tube was then sealed and stirred at 90 °C for 72 h. The mixture was cooled to room temperature and filtered. The solvent was removed under reduced pressure. The mixture was then diluted with CH_2Cl_2 and water, and the organic phase was collected and washed consecutively with water. The organic layer was dried over $NaSO_4$ and concentrated. The crude product was purified by column chromatography on silica gel first using ethyl acetate/hexane (3:2) and then ethyl acetate/hexane (4:1) as an eluent to yield 0.42 g of a yellow solid (52% yield, mp =116−117 °C). ^{1}H NMR (500 MHz, $CDCl_3$) δ: 7.61 (d, J = 8 Hz, 2H), 7.54 (s, 2H), 7.48 (m, 6H), 7.13 (d, J = 16 Hz, 2H), 7.04 (d, J = 16 Hz, 2H), 6.94 (d, J = 8.5 Hz, 4H), 3.61 (t, J = 5.5 Hz, 8H), 3.41 (m, 8H), 3.33 (m, 12H), 2.82 (t, J = 6.5 Hz, 4H), 2.47 (t, J = 7.5 Hz, 4H), 1.49 (s, 18H), 1.12 (t, J = 7 Hz, 6H). ^{13}C NMR (125 MHz, $CDCl_3$) δ: 154.7, 150.5, 149.6, 139.4, 136.9, 129.3, 127.9, 127.5, 126.3, 125.9, 120.5, 119.8, 116.3, 79.9, 70.0, 69.6, 67.0, 66.5, 50.9, 48.9, 39.9, 28.4, 15.0 ppm. HRMS (ESI-TOF) for $C_{59}H_{78}N_4O_8$ theoretical m/z $[M + H]^+$ = 971.5819; found $[M + H]^+$ = 971.5893.

2.2. Linear Photophysical and Photochemical Characterization and Computational Details. Comprehensive investigations of the steady-state linear absorption, fluorescence, and excitation anisotropy spectra and the fluorescence lifetimes and photochemical stability of **1** were conducted in hexane (HEX), toluene (TOL), chloroform ($CHCl_3$), tetrahydrofuran (THF), and acetonitrile (ACN) at room temperature. All the solvents were of spectroscopic grade and used as received. The steady-state linear absorption spectra were obtained with an Agilent 8453 UV−visible spectrophotometer in 10 mm path length quartz cuvettes for dye concentrations of C ≈ (1.6−2) × 10^{-5} M. The steady-state fluorescence and excitation anisotropy spectra were measured in the photon-counting regime using a PTI QuantaMaster spectrofluorimeter and 10 mm spectrofluorometric quartz cuvettes with C ≈ 10^{-6} M. All fluorescence spectra were corrected for the spectral response of the PTI detection system. The steady-state excitation anisotropy spectra of **1** were measured in the "L-format" configuration[35] with the extraction of a weak solvent emission and scattered light. The values of the experimentally observed excitation anisotropy can be expressed as[35]

$$r = r_0/(1 + \tau/\theta) \approx r_0 \quad (1)$$

where r_0 is the fundamental anisotropy; $\theta = \eta V/(kT)$ is the rotational correlation time (η, V, k, and, T are the solvent viscosity, effective rotational molecular volume, Boltzmann's constant, and absolute temperature, respectively); τ is the molecular fluorescence lifetime. The value of r_0 was determined in viscous polyTHF (pTHF), where $\theta \gg \tau$ for typical organic molecules, so $r \approx r_0$. Fluorescence quantum yields of **1**, Φ, were measured in solutions with C ≈ 10^{-6} M by a standard method relative to 9,10-diphenylanthracene in cyclohexane.[35] The values of the fluorescence lifetimes of **1**, τ, were determined with a time-correlated single photon-counting system, PicoHarp 300, under linear polarized femtosecond excitation,

dx.doi.org/10.1021/jp302274v | J. Phys. Chem. C 2012, 116, 11261−11271

oriented by the magic angle, and with a total time resolution of ~80 ps.

The photochemical stability of **1** in the employed organic solvents was investigated under linear excitation with a UV-lamp (LOCTITE 97034, excitation wavelength, $\lambda_{ex} \approx 405$ nm, average irradiance ~90 mW/cm^2). The photodecomposition quantum yields, Φ_{Ph}, were obtained as[36]

$$\Phi_{Ph} = \frac{[D(\lambda, 0) - D(\lambda, t_{ir})]N_A}{10^3 \cdot \varepsilon(\lambda) \cdot I(\lambda) \cdot \int_0^{t_{ir}} [1 - 10^{-D(\lambda,t)}]dt} \quad (2)$$

where $D(\lambda,t)$, $\varepsilon(\lambda)$, N_A, $I(\lambda)$, and t_{ir} are the optical density of solution at wavelength, λ, and time, t, extinction coefficient (in $M^{-1}\cdot cm^{-1}$), Avogadro's number, laser irradiance (in photon$\cdot cm^{-2}\cdot s^{-1}$), and total irradiation time, respectively. A comprehensive description of this absorption methodology was described previously.[36,37]

The electronic properties of **1** were also investigated by quantum chemical calculations using HyperChem V7.0 for Windows. The ground-state geometry optimization was performed by the AM1 method and was stopped upon reaching a gradient of 0.01 kcal/mol. The semiempirical ZINDO/S method with the 10 highest-occupied molecular orbitals (HOMO) and 10 lowest-unoccupied molecular orbitals (LUMO) was used for the calculation of the electronic spectrum of **1** in a vacuum. The values of the average overlap weighting factors, 1.267 and 0.55, were used for σ and π bonds, respectively, to obtain acceptable agreement between the calculated and experimentally observed energies of the long wavelength absorption maximum of **1**. The changes in the π weighting factor from 0.47 to 0.59 did not significantly alter the relative positions of the calculated energies of the electronic levels.

2.3. Transient Absorption, 2PA, and Superfluorescence Measurements. The investigation of the excited-state dynamic processes in **1** was performed with a femtosecond laser system (Coherent, Inc.), schematically shown in Figure 1. The output of a self-mode-locking Ti:sapphire laser (Mira 900-F, 800 nm exit wavelength, average power ~1.1 W, pulse duration $\tau_P \approx 200$ fs, and repetition rate $f = 76$ MHz), pumped by the second harmonic of cw Nd^{3+}:YAG laser (Verdi-10), was regeneratively amplified (Legent Elite USP) providing ~100 fs pulses (fwhm) with energy ~3.6 mJ/pulse and a 1-kHz repetition rate. This output was split into two separate beams with an average power ~1.8 W and pumped two ultrafast optical parametric amplifiers [OPerA Solo (OPA)] with a broad tuning range 0.24−20 μ, $\tau_P \approx 100$ fs (fwhm), and pulse energies $E_P \leq 100$ μJ. The transient excited-state absorption measurements were performed based on the pump−probe technique[38,39] with two femtosecond laser beams from the separate OPA systems simultaneously pumped at 800 nm, as shown in Figure 1. The first (pump) beam from OPA with $E_P \approx 1.0-1.3$ μJ, $\tau_P \approx 100$ fs (fwhm), and $f = 1$ kHz was tuned to 400 nm and used as a one-photon excitation source for investigation solutions. The second (probe) beam from another OPA with $E_P \leq 5$ nJ and $\tau_P \approx 100$ fs (fwhm) was delayed in time by a optical line (M-531.DD, PI, Inc.) with a retroreflector and tuned into the spectral range of 440−700 nm. The pump and probe laser beams, with a nearly Gaussian space profile and linear polarizations oriented by the magic angle, were focused to the waists of radii ~0.3 mm and ~0.1 mm, respectively, and recombined at a small angle (<5°) in a 1 mm path length flow cell with the sample solution. The flow rate of ~200 mL/min excluded the influence of any accumulative effects in the sample solutions on the obtained data under the employed experimental conditions. The optical density of the investigated media was set to be ~0.6−0.8 at the excitation wavelength. The temporal resolution of the used pump−probe technique was estimated at ≤300 fs from the analytical fitting of the rise-up portion of transient ESA dependencies with a 100 fs pump and probe Gaussian pulses.

The degenerate 2PA spectra of **1** were measured in TOL and ACN solutions by the direct open-aperture Z-scan[28] and relative 2PF[29] methods using a single laser beam from the first OPA (Figure 1). In the case of 2PF measurements, the same laser beam was coupled with a PTI QuantaMaster spectrofluorimeter, and Rhodamine B in methanol and Fluorescein in water (pH = 11) were used as standards.[40] The quadratic dependence of the integral 2PF signal on the excitation power was confirmed for each λ_{ex}.

The superfluorescence properties of **1** were investigated in TOL and ACN solutions with dye concentrations in the range 10^{-4} M ≤ C ≤ 3×10^{-3} M under femtosecond transverse pumping at $\lambda_{ex} = 400$ nm. Sample solutions were placed in 4 × 10 × 35 mm spectrofluorometric quartz cells and transversely pumped by a 1-kHz femtosecond pulse train with $\tau_P \approx 100$ fs (fwhm) and $E_P \leq 4.5$ μJ. The pump beam was focused by a cylindrical lens to the waist of 0.2 × 4 mm, and the intensity and spectral shapes of a superfluorescence emission of **1** were measured in the perpendicular direction by an HR4000 fiber optic spectrometer (Ocean Optics, Inc.).

2.4. Bioimaging. *Cell Culture and Incubation.* HCT 116 cell (purchased from America Type Culture Collection, Manassas, VA) were cultured in RPMI-1640, supplemented with 10% fetal bovine serum, and 1% penicillin, 1% streptomycin, at 37 °C, in a 95% humidified atmosphere containing 5% CO_2. No. 1 round 12 mm coverslips were treated with poly-D-lysine, to improve cell adhesion, and washed (3×) with a phosphate-buffered saline (PBS) buffer solution. The treated coverslips were placed in 24-well plates and 40,000 cells/well were seeded and incubated for 36 h before incubation with the dye. From a 800 μM stock solution of probe **1** in DMSO, a 20 μM solution in culture medium was prepared, as well as a 75 nM solution of LysoTracker Red (Invitrogen). These solutions were used to incubate the cells for 1 h. After incubation, cells were washed with PBS three times, fixed with 3.7% formaldehyde in PBS at room temperature for 10 min, and incubated twice with $NaBH_4$ (1 mg/mL) in PBS at room temperature for 10 min. The cells were then washed with PBS twice and mounted on microscopy slides with Prolong Gold (Invitrogen) mounting media for imaging.

One- and Two-Photon Fluorescence Imaging. One-photon and two-photon fluorescence images were recorded on a Leica TCS SP5 II laser-scanning confocal microscope system. For one-photon imaging, cells were excited at 405 nm. Fluorescence emission was collected from 450 to 550 nm. The confocal pinhole was applied for better image quality. Two-photon fluorescence imaging was recorded on the same Leica TCS SP5 microscope system coupled to a tunable Coherent Chameleon Vision S (80 MHz, mode-locked, 75 fs pulse width, tuned to 700 nm). Two-photon induced fluorescence was collected with a water immersion 63× objective (HCX Pl APO CS 63.0 × 1.20 WATER UV).

Table 1. Steady-State Absorption λ_{abs}^{max} and Fluorescence λ_{fl}^{max} Maxima, Stokes Shifts, Maxima Extinction Coefficients ε^{max}, Fluorescence Quantum Yields Φ, Experimental τ and Calculated τ_{cal} Fluorescence Lifetimes, and Photobleaching Quantum Yields Φ_{Ph} of 1 in Organic Solvents with Different Polarity Δf and Room Temperature Viscosity η

N/N	HEX	TOL	$CHCl_3$	THF	ACN
λ_{abs}^{max}, nm	389 ± 1	398 ± 1	397 ± 1	397 ± 1	394 ± 1
λ_{fl}^{max}, nm	432 ± 1	452 ± 1	483 ± 1	490 ± 1	530 ± 1
Stokes shift, cm^{-1} (nm)	2560 ± 100 (43 ± 2)	3000 ± 100 (54 ± 2)	4490 ± 100 (86 ± 2)	4780 ± 100 (93 ± 2)	6510 ± 100 (136 ± 2)
$\varepsilon^{max} \times 10^{-3}$, $M^{-1}\cdot cm^{-1}$	89 ± 7	81 ± 7	79 ± 7	81 ± 7	90 ± 7
Φ	0.88 ± 0.05	1.0 ± 0.05	1.0 ± 0.05	1.0 ± 0.05	0.94 ± 0.05
τ^a, ns	0.89 ± 0.08	1.00 ± 0.08	1.29 ± 0.08	1.40 ± 0.08	1.76 ± 0.08
τ_{cal}, ns	1.06 ± 0.1	1.25 ± 0.1	1.5 ± 0.1	1.6 ± 0.1	1.78 ± 0.1
$\Phi_{Ph} \times 10^4$	8 ± 1	1.3 ± 0.2	68 ± 10	2.6 ± 0.4	28 ± 4
Δf^b	3×10^{-4}	0.0135	0.148	0.209	0.305
η, cP	0.31	0.59	0.54	0.48	0.34

[a]These data were obtained with a goodness-of-fit parameter $\chi^2 \geq 0.99$. [b]Orientation polarizability $\Delta f = (\varepsilon-1)/(2\varepsilon+1) - (n^2-1)/(2n^2+1)$ (ε and n are the dielectric constant and refraction index of the solvent, respectively).

3. RESULTS AND DISCUSSION

3.1. Linear Photophysical and Photochemical Properties of 1. Fluorene **1** was selected for study due to its relatively long π-electron conjugation, reasonably high molecular symmetry, ability to be functionalized to impart hydrophilicity (for potential 2PFM imaging), and introduced additional biomarker targeting functionality in the *N*-phenylpiperazine moiety. The main photophysical and photochemical parameters of **1** along with its steady-state absorption and fluorescence spectra in a number of aprotic solvents are presented in Table 1 and Figure 2. A structureless spectral shape and a weak dependence on solvent properties were observed for the steady-state absorption spectra of **1** in all investigated solutions. These spectra were independent of molecular concentration up to C ≈ 10^{-2} M and nicely overlapped with the corrected excitation spectra of **1**, which is indicative of negligible aggregation effects and spectral independence of the fluorescence quantum yields, Φ, respectively. The relatively large values of the extinction coefficients of **1**, $\varepsilon^{max} \approx (80-90) \times 10^{-3}$ $M^{-1}\cdot cm^{-1}$ (Table 1), determine the efficient one-photon transition dipoles $S_0 \rightarrow S_1$[41]

$$\mu_{01} = \sqrt{\frac{1500\cdot(\hbar c)^2\cdot\ln(10)}{\pi\cdot N_A\cdot E_{01}}\cdot\int\varepsilon_{01}(\nu)d\nu} \approx 11.8 - 12.5\text{D} \quad (3)$$

where S_0, S_1, $\hbar$, c, and $\varepsilon(\nu)$ are the ground and first excited electronic states, Planck's constant, velocity of light in a vacuum, and extinction coefficient (in $M^{-1}\cdot cm^{-1}$) at the wavenumber ν (in cm^{-1}), respectively; E_{01} is the energy of the $S_0 \rightarrow S_1$ electronic transition. The steady-state fluorescence spectra of **1** were independent of the excitation wavelength in the whole absorption range and exhibited strong solvatochromic behavior and a well-defined vibrational structure in nonpolar solvents (Figure 2, curves 1′−5′). The dependence of the Stokes shift on solvent polarity, Δf, was in good agreement with the Lippert equation (Figure 3a), which is indicative of the dominant role of general solute−solvent interactions. The large values of Stokes shifts (up to ~140 nm) and noticeable changes in the shape of the fluorescence spectra observed for symmetrical molecule **1** are typical for donor−acceptor fluorenes with extended π-conjugation[9,42] and can be

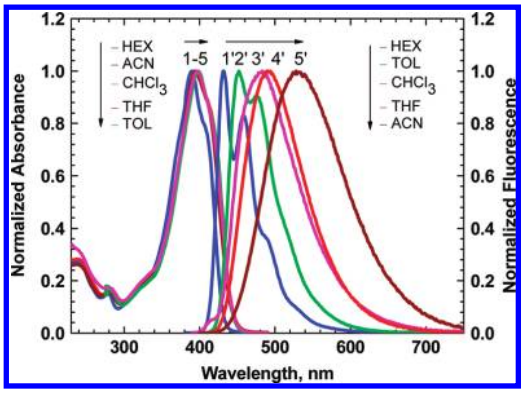

Figure 2. Normalized steady-state absorption (1−5) and fluorescence (1′−5′) spectra of **1** in hexanes (HEX) (1, 1′), toluene (TOL) (5, 2′), $CHCl_3$ (3, 3′), THF (4, 4′), and acetonitrile (ACN) (2, 5′).

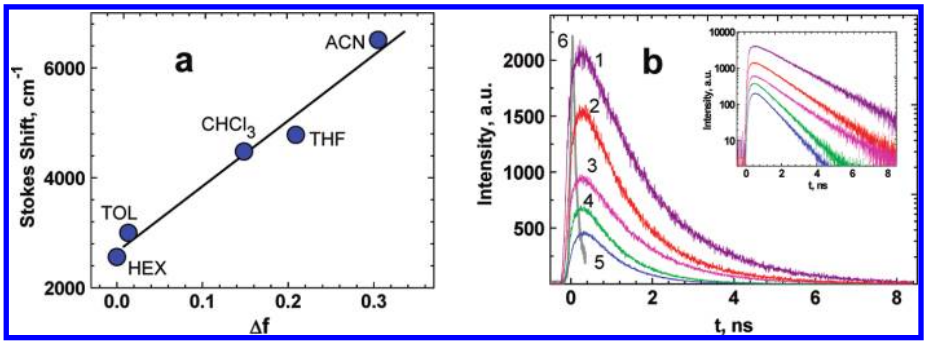

Figure 3. (a) Lippert dependence for **1**. (b) Fluorescence decay curves for **1** in HEX (1), TOL (2), $CHCl_3$ (3), THF (4), ACN (5), and instrument response function (6). Inset represents the log scale of the fluorescence decay curves.

dx.doi.org/10.1021/jp302274v | J. Phys. Chem. C 2012, 116, 11261−11271

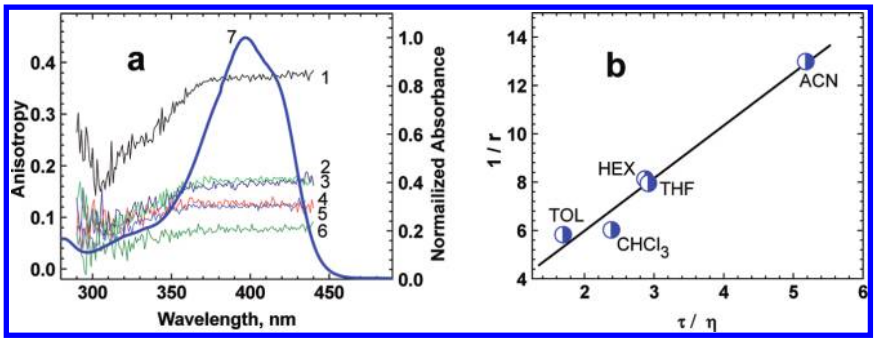

Figure 4. (a) Steady-state excitation anisotropy spectra of **1** in pTHF (1), TOL (2), $CHCl_3$ (3), THF (4), HEX (5), ACN (6), and a normalized absorption spectrum in THF (7). (b) Experimental dependence $1/r = f(\tau/\eta)$ for the investigated solutions of **1**.

explained by the effect of symmetry-breaking in the S_1 state after electronic excitation.[43]

High fluorescence quantum yields of **1** ($\Phi \approx 0.88-1.0$) were observed in all the solvents used, and no dependence on the excitation wavelength was found over a broad spectral range. Fluorescence decay processes in **1** corresponded to a single-exponential profile (Figure 3b) with $\tau \approx 0.9-1.8$ ns (Table 1) and a monotonic increase in τ with solvent polarity was observed. The values of the calculated fluorescence lifetimes of **1** were determined from the equation $\tau_{cal} = \tau_N \cdot \Phi$, where the natural lifetime, τ_N, can be expressed as[35]

$$1/\tau_N = 2.88 \cdot 10^{-9} \cdot n^2 \cdot \frac{\int F(\nu) d\nu}{\int [F(\nu)/\nu^3] d\nu} \cdot \int [\varepsilon(\nu)/\nu] d\nu \quad (4)$$

where $F(\nu)$ is the quantum fluorescence intensity. An acceptable agreement between the experimental, τ, and calculated, τ_{cal}, lifetimes was observed (Table 1), which also confirms the dominant role of general solute−solvent interactions.

The steady-state excitation anisotropy spectra of **1** (Figure 4a, curves 1−6) reveal the nature of the main long wavelength absorption band (curve 7). The experimental dependencies $r(\lambda_{ex})$ exhibited nearly constant values of anisotropy in the spectral range 360 nm $\leq \lambda_{ex} \leq$ 440 nm, which is evidence that a single electronic transition, $S_0 \rightarrow S_1$, was responsible for the main absorption band of **1** in all investigated solvents. In relatively viscous pTHF $r \approx r_0$ ($\theta \gg \tau$), the maximum fundamental anisotropy value $r_0 \approx 0.38$ was close to the theoretical limit,[35] which is indicative of the nearly parallel orientation of the absorption, $\boldsymbol{\mu}_{01}$ ($S_0 \rightarrow S_1$), and emission, $\boldsymbol{\mu}_{10}$ ($S_1 \rightarrow S_0$), transition dipoles in accordance with the equation[35] $r_0 = (3\cos^2\alpha - 1)/5 \approx 0.38$ ($\alpha \approx 10°$ is the angle between $\boldsymbol{\mu}_{01}$ and $\boldsymbol{\mu}_{10}$). In low viscosity solvents, the values of excitation anisotropy monotonically decreased with increasing $1/\eta$ due to molecular rotational processes. As follows from eq 1, the nearly linear experimental plot of $1/r = f(\tau/\eta)$ (Figure 4b) is indicative of a weak dependence of the fundamental value r_0 and effective rotational volume V on solvent properties. The estimation of the effective size of the rotational molecular volume gives a relatively large value, $V \approx 6200$ Å^3, allow one to assume an important role for the alkyl groups in the formation of the volumetric shape of the molecular solvate cage.

The kinetics of the photodecomposition processes of **1** revealed a dominant role of the first-order photoreactions in all the investigated solvents, and the corresponding photochemical decomposition quantum yields, Φ_{Ph}, were in the range of $\sim(1.3-68) \times 10^{-4}$ (Table 1). The highest photostability of **1** was observed in toluene. It should be mentioned that the obtained values of Φ_{Ph} are somewhat larger than other reported fluorene derivatives,[36,37] but are reasonable for use in fluorescence microscopy.

3.2. Calculated Electronic Properties of 1. A simple quantum-chemical analysis of the electronic structure of **1** was performed using HyperChem V7.0 for Windows. The optimized molecular geometry and main electronic parameters of **1**, including the orbital configurations and oscillator strengths of the electronic transitions, are presented in Figure 5 and Table 2, respectively. As follows from these data, the

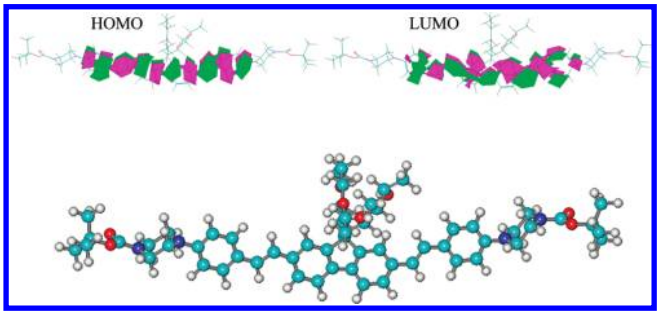

Figure 5. Optimized molecular geometry, HOMO and LUMO orbitals of **1**.

Table 2. Values of the Calculated Energies of the Electronic Transitions, E_{0i}, Oscillator Strengths, f_{OS}, and Transition Dipoles, μ_{0i}, of 1

transition	E_{0i}, nm (eV)	f_{OS}	μ_{0i}, D	main configuration
$S_0 \rightarrow S_1$	397.2 (3.1)	2.60	14.82	0.93 |HOMO→LUMO⟩
$S_0 \rightarrow S_2$	322.4 (3.85)	0.092	2.51	−0.78 |HOMO→ LUMO +1⟩ 0.58 |HOMO−1→ LUMO⟩
$S_0 \rightarrow S_3$	303.7 (4.08)	0.0012	0.28	0.62 |HOMO→ LUMO+7⟩ −0.50 |HOMO−5→ LUMO⟩
$S_0 \rightarrow S_4$	300.3 (4.13)	0.0172	1.05	0.45|HOMO→ LUMO+2⟩ 0.51 |HOMO→ LUMO +8⟩
$S_0 \rightarrow S_5$	284.3 (4.36)	0.0623	1.94	0.50 |HOMO→ LUMO+4⟩

calculated electronic spectrum of **1** is sufficiently close to the corresponding linear absorption ones (Figure 2), and the first electronic transition is determined mainly by one pure configuration (HOMO → LUMO). It should be mentioned that the first five ground-state electronic transitions ($S_0 \rightarrow S_n$, n = 1−5) are of the $\pi-\pi$ type and exhibit large differences in the space orientation of their transition dipoles when the angles

dx.doi.org/10.1021/jp302274v | J. Phys. Chem. C 2012, 116, 11261−11271

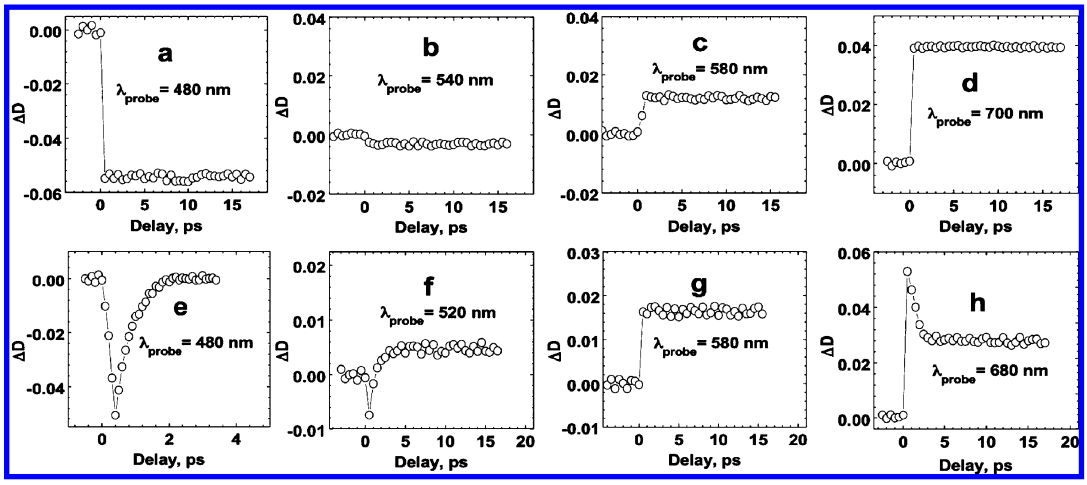

Figure 6. Transient absorption signals $\Delta D = f(\tau_D)$ at different probe wavelengths, λ_{probe}, for **1** in TOL [λ_{probe} = 480 nm (a); 540 nm (b); 580 nm (c); 700 nm (d)] and ACN [λ_{probe} = 480 nm (e); 520 nm (f); 580 nm (g); 680 nm (h)].

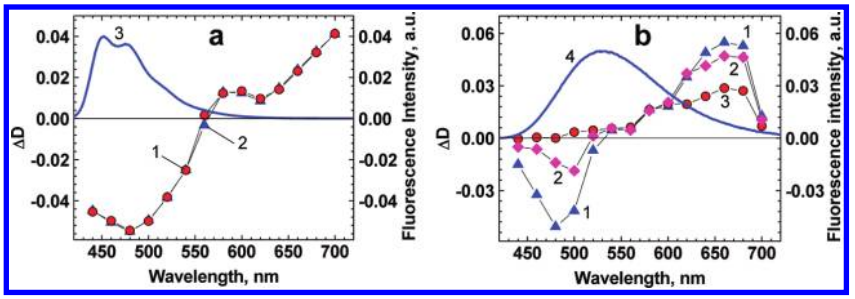

Figure 7. Time-resolved ESA spectra of **1** in TOL [(a) τ_D = 0.5 ps (1) and 20 ps (2)] and in ACN [(b) τ_D= 0.5 ps (1), 1 ps (2), and 20 ps (3)]. Steady-state fluorescence spectra in TOL [(a), curve 3] and ACN [(b), curve 4].

between $\boldsymbol{\mu}_{01}$ and $\boldsymbol{\mu}_{0i}$ (i = 2−5) are close to 0 or 90°. This is expected for symmetrical type molecules. Presumably, the minimum value of the fundamental anisotropy at $\lambda_{ex} \approx$ 305 nm (Figure 4a, curve 1) is close to the spectral position of the $S_0 \rightarrow S_4$ transition, which is qualitatively reflected in the decreasing fluorescence anisotropy in the spectral range of $\lambda_{ex} \leq$ 360 nm. The oscillator strength of the third transition is sufficiently small ($f_{OS} \approx$ 0.0012), so it is possible to assume that this transition can be active in 2PA processes.

3.3. Transient Gain and ESA Spectra of 1. The dynamic processes in the excited state of **1** were investigated using a femtosecond pump−probe technique (Figure 1) in the TOL and ACN solutions at room temperature. The kinetics of the transient gain and ESA signals, $\Delta D = f(\tau_D)$ (ΔD is the induced change in the optical density of the solution and τ_D is the time delay between the pump and probe pulses), at different probe wavelengths and the obtained time-resolved gain and ESA spectra of **1** are presented in Figures 6 and 7, respectively. According to parts a−d of Figure 6 and Figure 7a, in nonpolar TOL, the pumping pulse produced a long-lived gain band (negative ΔD) in the spectral range 440−560 nm, which overlaps nicely with the steady-state fluorescence contour of **1** and relaxed to zero in accordance with the lifetime of the S_1 state (∼ 1 ns). The ESA band (positive ΔD) was observed for $\lambda_{probe} \geq$ 580 nm and also relaxed to zero in the nanosecond time scale. Taking into account the time resolution of the experimental system (∼300 fs), this means that in nonpolar TOL all vibrational (Franck−Condon)[35] and solvate relaxation processes for **1** were finished in less than 500 fs. It should be mentioned that the typical time of solvent relaxation processes resulting in the well-known red shift of the instantaneous fluorescence spectrum is up to 5−100 ps in low-viscosity dye solutions.[35,44] Presumably, in a nonpolar medium, the solvent−solute interaction should be weak, so this solvent relaxation process was not observed in transient absorption kinetics. As seen in Figure 7a, the superfluorescence and lasing effects in the TOL solution of **1** can be expected in the spectral range of the gain band, 440−560 nm. In contrast, the behavior of **1** in the polar ACN solution revealed picosecond gain and ESA relaxation processes (parts e−h of Figure 6 and Figure 7b). Presumably, in this case, the vibrational Franck−Condon relaxation should be completed in ∼500 fs when the maxima transient signals arise. After that, a fast (∼1−2 ps) relaxation process occurs, which is reflected in the spectral behavior of the transient gain and ESA bands (Figure 7b). The nature of this relatively fast relaxation can be attributed to the symmetry-breaking effect in the excited S_1 state of **1**.[43] It seems that another possible explanation for this phenomenon based on the atypically fast solvent relaxation process is less probable. The red shift and narrowing of the instantaneous gain spectrum of **1** at 0.5 and 1 ps (Figure 7b, curves 1 and 2) confirm these assumptions. The short-lived gain band at 480−500 nm can be considered as a potential source of light amplification in the superfluorescence and lasing phenomena of **1** in polar ACN.

3.4. 2PA Spectra of 1. The degenerate 2PA spectra of symmetrical compound **1** were investigated in TOL (nonpolar) and ACN (polar) solutions by two independent open-aperture Z-scan[28] and 2PF[29] methods and are presented in Figure 8. The values of the 2PA cross sections, δ_{2PA}, were obtained by these two techniques and eq 5

dx.doi.org/10.1021/jp302274v | J. Phys. Chem. C 2012, 116, 11261−11271

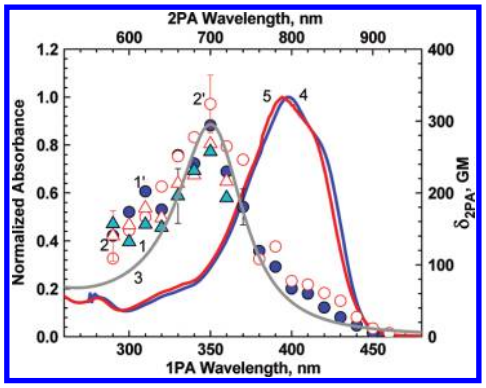

Figure 8. Degenerate 2PA spectra of **1** in TOL (1, 1′) and ACN (2, 2′), obtained by open-aperture Z-scan (1, 2, triangles) and 2PF (1′, 2′, circles) methods and the best fit (3) by eq 5. Normalized steady-state absorption spectra of **1** in TOL (4) and ACN (5).

$$\delta_{2PA} \approx \frac{64\pi^4}{15c^2h^2n^2}\left[\frac{\nu_{ex}^2|\boldsymbol{\mu}_{01}|^2|\boldsymbol{\mu}_{1f}|^2}{E^2+\Gamma_{01}^2}(1+2\cos^2\beta)\right]\cdot g(2\nu_{ex}) \quad (5)$$

where $\boldsymbol{\mu}_{01}$, and $\boldsymbol{\mu}_{1f}$ are the transition dipole moments for the $S_0 \rightarrow S_1$ and $S_1 \rightarrow S_f$ electronic transitions, respectively (S_f is the final electronic state for the two-photon transition); $E = hc\cdot(1/\lambda_{ab}^{max} - 1/\lambda_{ex})$; $\nu_{ex} = c/\lambda_{ex}$; Γ_{01} is the damping constant related to the transition frequency $\nu_{01} = c/\lambda_{ab}^{max}$; β is the angle between vectors $\boldsymbol{\mu}_{01}$ and $\boldsymbol{\mu}_{1f}$; and $g(2\nu_{ex})$ is the normalized Lorentzian shape function. The best fit curve of the experimental 2PA spectra of **1** (Figure 8, curve 3) was obtained by eq 5 with the parameters $\boldsymbol{\mu}_{01}$ = 14.5 D, Γ_{01}= 0.2 eV, $\boldsymbol{\mu}_{1f}$ = 10 D, Γ_{0f} = 0.25 eV, and β = 0, which were in good agreement with the corresponding values obtained from quantum-chemical calculations and separate experimental methods. The high fluorescence quantum yield, acceptable 2PA cross sections, and photochemical stability afford a relatively high figure of merit,[3] $F_M = \Phi\cdot\delta_{2PA}/\Phi_{Ph} \approx 10^5-10^6$, which is comparable with typical fluorescence labels[3,10] and reflect good prospects of **1** for use in 2PFM.

The separate techniques were in relatively good agreement with each other in the overlapping spectral range of 580−720 nm. The 2PA spectra of **1** exhibited only one well-defined band at ∼350 nm and monotonic decrease in the long wavelength one-photon absorption contour, which is typical of symmetrical fluorene derivatives.[36,45] The maxima values of δ_{2PA} were ∼300 GM, and no strong dependence of 2PA efficiency on solvent polarity was observed. Taking into account the extremely small changes in the stationary dipole moment for symmetrical type compounds that occur under electronic excitation (∼0.01−0.5 D), the nature of 2PA processes in **1** can be analyzed based on the expression for the simplified three-level electronic model.[46]

3.5. Superfluorescence Properties of 1. The introduction of the superfluorescence and lasing phenomena of the fluorescence probes into the fluorescence microscopy technique potentially can be used for further improvements of the image quality based on a dramatic decrease in emission lifetimes and an increase in spectral brightness. The superfluorescence parameters of **1** were investigated under femtosecond transverse pumping in the main absorption band (λ_{ex} = 400 nm) in solutions of different polarity (TOL, ACN) with dye concentrations 10^{-4} M ≤ C ≤ 3×10^{-3} M (Figures 9−11). In relatively low-concentration TOL solutions (∼10^{-4} M) the

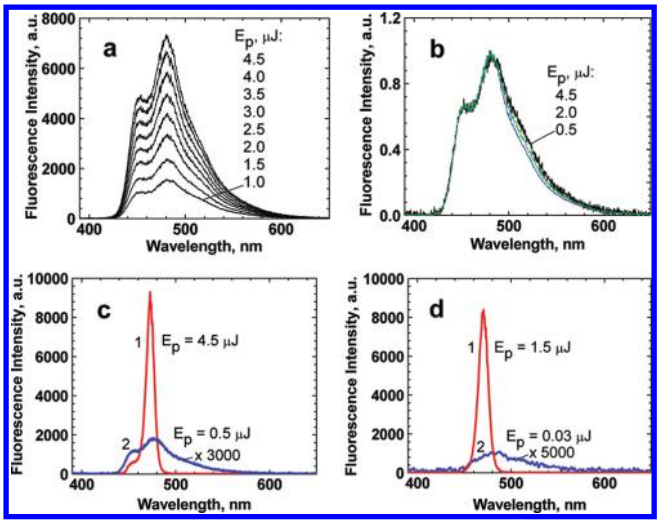

Figure 9. Fluorescence emission and superfluorescence spectra of **1** in TOL solutions. (a) Fluorescence spectra under femtosecond pulsed excitation with corresponding pulse energies: E_P = 1.0−4.5 μJ and C ≈ 10^{-4} M. (b) Normalized fluorescence spectra for E_P = 0.5 μJ (black), 2.0 μJ (green), 4.5 μJ (blue), and C ≈ 10^{-4} M. (c) Superfluorescence spectrum (1) for E_P = 4.5 μJ (red), fluorescence spectrum (2) for E_P = 0.5 μJ (blue), and C ≈ 5×10^{-4} M. (d) Superfluorescence spectrum (1) for E_P = 1.5 μJ (red) and fluorescence spectrum (2) for E_P = 0.03 μJ (blue) and C ≈ 2.8×10^{-3} M.

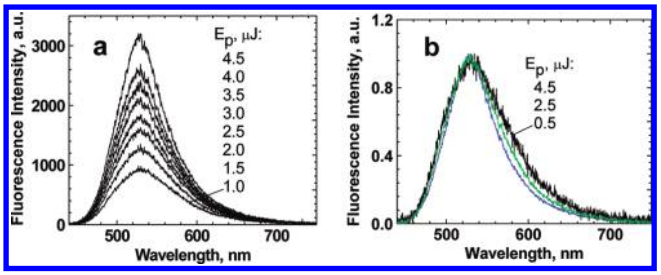

Figure 10. Fluorescence spectra of **1** in ACN solution with C ≈ 3×10^{-3} M under femtosecond pulsed excitation. (a) Fluorescence spectra for corresponding pulse energies: E_P = 1.0−4.5 μJ. (b) Normalized fluorescence spectra for E_P = 0.5 μJ (black), 2.5 μJ (green), and 4.5 μJ (blue).

intensity of the spontaneous fluorescence emission of **1** increased linearly with the pump pulse energy, and a small narrowing in the fluorescence band was observed (parts a and b of Figure 9 and Figure 11). It should be mentioned that the spectral shape of these fluorescence spectra deviated from the corresponding one in Figure 2 due to the effect of reabsorption. The increase in concentration, up to 5×10^{-4} M, resulting in the efficient superfluorescence of **1** in TOL and corresponding amplified stimulated emission spectra are presented in curve 1 of parts c and d of Figure 9.

The spectral width of the superfluorescence spectra (∼10−15 nm) was much narrower than the regular steady-state fluorescence spectra (curves 2) and close to the corresponding parameters of typical dye lasers.[47] In contrast to some potential possibility of amplification in the fluorescence spectral range (see gain spectra in Figure 8b, curves 1 and 2) in polar ACN solutions of **1**, no superfluorescence phenomena were observed even for the highest molecular concentration ∼3×10^{-3} M and maximum excitation energy $E_P \approx 4.5$ μJ (Figure 10a). Only a small narrowing in the fluorescence band was observed (Figure 10b), as in a nonpolar TOL for low-concentrated solutions. In

dx.doi.org/10.1021/jp302274v | J. Phys. Chem. C 2012, 116, 11261−11271

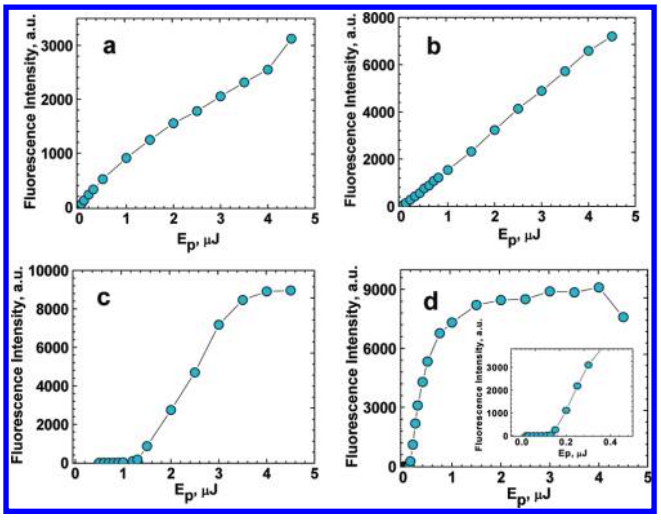

Figure 11. Dependencies of fluorescence intensity on excitation pulse energy E_P for **1** in ACN (a) and TOL (b-d) solutions with dye concentrations C ≈ 3×10^{-3} M (a), 1×10^{-4} M (b), 5×10^{-4} M (c), and 2.8×10^{-3} M (d) under femtosecond transverse pumping at 400 nm.

this case, a nearly linear dependence of the integral fluorescence intensity on E_P was observed (Figure 11a). In contrast to polar ACN, concentrated TOL solutions of **1** (C ≥ 5×10^{-4} M) exhibited efficient superfluorescence emission with the typical threshold dependencies of superfluorescence intensity on E_P (parts c and d of Figure 11). The lowest threshold of ∼15−20 $\mu J/cm^2$ was observed for C ≈ 3×10^{-3} M, which is comparable with the corresponding parameters of the pulsed laser system.[48−50]

3.6. Fluorescence Bioimaging. The potential utility of probe **1** for 2PFM cellular imaging was demonstrated and uptake of **1** by HCT 116 cells was evaluated. Viability assays in an epithelial colorectal carcinoma cell line, HCT 116, were conducted via the MTS assay (Figure S1 of Supporting Information shows the viability data for HCT 116 cells after treatment with several concentrations of probe **1** for 24 h). The data indicate that probe **1** has low cytotoxicity over a concentration range from 1 to 25 μM, appropriate for cell imaging. The one-photon fluorescence microscopy (1PFM) and 2PFM images showed that **1** can be effectively taken up by HCT 116 cells. To determine the location of the probe **1** in the cell, a colocalization study of **1** with well-known lysosomal selective dye (Lysotracker Red) in HCT 116 cells was conducted. One-photon fluorescence images, collected for Lysotracker Red and probe **1**, are shown in parts b and c of Figure 12, respectively, as well as the differential interference contrast (DIC) image (Figure 12a), along with the overlap image of a, b, and c (Figure 12d). As shown in Figure 12d, the colocalization of both probes suggests similar uptake for both the Lysotracker dye and probe **1**. Pearson's correlation coefficient was calculated within Slidebook 5.0, image processing software. The correlation coefficient of probe **1** relative to LysoTrackerRed was >0.87 supporting lysosomal colocalization, consistent with previous reports.[51,52] 2PFM imaging (Figure 13c) revealed remarkable contrast when compared to the one-photon fluorescence (Figure 13b), further supporting the potential of this probe in bioimaging applications.

4. CONCLUSIONS

The synthesis and comprehensive characterization of linear photophysical, excited-state dynamics, 2PA, and superfluorescence properties of a new probe (**1**) in a number of organic solvents were presented. Ground-state linear absorption spectra of **1** revealed a weak dependence on solvent properties, typical of fluorene derivatives. In spite of the symmetrical structure of the new fluorene, its fluorescence emission spectra exhibited strong solvatochromic behavior with a maximum Stokes shift up of to ∼140 nm in ACN, which can be explained by the symmetry-breaking effect in the first excited state of **1**. High fluorescence quantum yields (∼0.9−1.0) and a single exponential decay in the fluorescence emission of **1** were observed in all the solvents investigated, and good agreement between experimental and calculated fluorescence lifetimes was obtained. The excitation anisotropy spectra of **1** revealed the nature of the main long wavelength absorption band, which is related with only one electronic transition, $S_0 \rightarrow S_1$ and were in good agreement with the results of semiempirical quantum chemical calculations. Excited-state dynamic properties of **1** were investigated using the femtosecond pump−probe technique in solvents of different polarity, while corresponding time-resolved ESA and gain spectra were obtained. Fast relaxation processes (∼1−2 ps) in the excited state of **1** were shown for polar ACN solutions, which may be associated with the symmetry-breaking effects in the fluorenyl structure upon electronic excitation. The degenerate 2PA spectra of symmetrical compound **1** were obtained over a broad spectral range by two independent methods, and only one well-defined two-photon allowed band was observed with a maximum cross-section, δ_{2PA} ≈ 300 GM. Photochemical decomposition quantum yields of **1** were measured in several solvents, and the highest figure of merit (F_M) values were in the range of ∼10^6. Significantly, efficient superfluorescence emission of **1** was observed in nonpolar TOL solutions under transverse pumping at 400 nm with the minimum threshold of ∼15−20

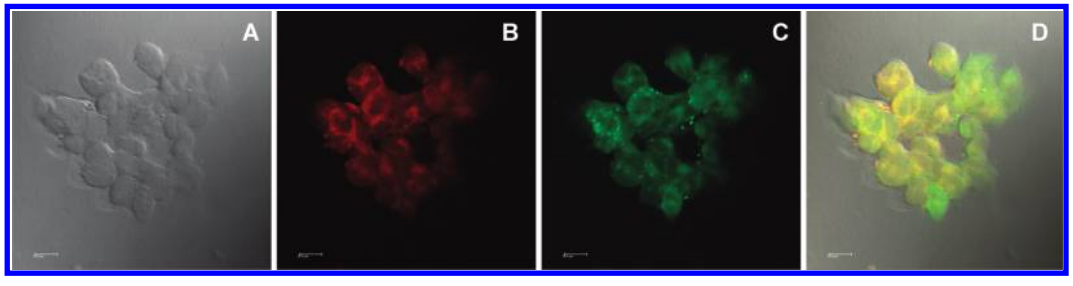

Figure 12. Confocal fluorescence images of HCT 116 cells incubated with 2PA probe **1** (20 μM, 1 h) and Lysotracker Red (75 nM, 1 h). DIC (a), one-photon fluorescence image showing Lysotracker Red (b) and probe **1** (c). (d) Colocalization (overlay of b and c). Scale bar is 10 μm.

dx.doi.org/10.1021/jp302274v | J. Phys. Chem. C 2012, 116, 11261−11271

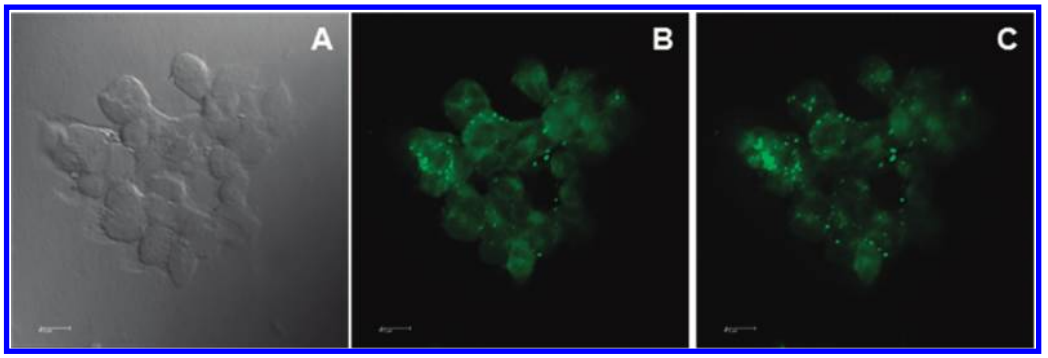

Figure 13. One-and two-photon fluorescence micrographs of HCT 116 cells incubated with probe **1** (20 μM, 1 h). DIC (a), one-photon fluorescence (b), and two-photon fluorescence images (c), 80 MHz, 75 fs pulse width tuned to 700 nm, 63× objective. Scale bar is 10 μm.

μJ/cm^2. The linear photophysical, photochemical, 2PA, and superfluorescence parameters of probe **1** is an important step in the development of new fluorescence labels with increased spectral brightness. Finally, the preliminary potential of probe **1** for applications in 2PFM was demonstrated via one- and two-photon fluorescence microscopy imaging of HCT 116 cells.

■ ASSOCIATED CONTENT

Supporting Information

Cell viability data for HCT 116 cells after incubation with several concentrations of probe **1** for 24 h. This material is available free of charge via the Internet at http://pubs.acs.org.

■ AUTHOR INFORMATION

Corresponding Author

*E-mail: belfield@ucf.edu.

Notes

The authors declare no competing financial interest.

■ ACKNOWLEDGMENTS

We wish to acknowledge the National Institute of Biomedical Imaging and Bioengineering of the National Institutes of Health (Grant No. 1 R15 EB008858-01), the National Academy of Sciences of Ukraine (Grant No. 1.4.1.B/153), the National Science Foundation (Grant Nos. ECCS-0925712, CHE-0840431, and CHE-0832622), and the National Academy of Sciences (Grant No. PGA-P210877) for their support of this work.

■ REFERENCES

(1) Denk, W.; Strickler, J. H.; Webb, W. W. *Science* **1990**, *248*, 73−76.
(2) Ding, J. B.; Takasaki, K. T.; Sabatini, B. L. *Neuron* **2009**, *63*, 429−437.
(3) Wang, X.; Nguyen, D. M.; Yanez, C. O.; Rodriguez, L.; Ahn, H.-Y.; Bondar, M. V.; Belfield, K. D. *J. Am. Chem. Soc.* **2010**, *132*, 12237−12239.
(4) Cumpston, B. H.; Ananthavel, S. P.; Barlow, S.; Dyer, D. L.; Ehrlich, J. E.; Erskine, L. L.; Heikal, A. A.; Kuebler, S. M.; Lee, I. Y. S.; McCord-Maughon, D.; Qin, J. Q.; Rockel, H.; Rumi, M.; Wu, X. L.; Marder, S. R.; Perry, J. W. *Nature* **1999**, *398*, 51−54.
(5) Kawata, S.; Kawata, Y. *Chem. Rev.* **2000**, *100*, 1777−1788.
(6) Belfield, K. D.; Ren, X. B.; Van Stryland, E. W.; Hagan, D. J.; Dubikovsky, V.; Miesak, E. J. *J. Am. Chem. Soc.* **2000**, *122*, 1217−1218.
(7) Dichtel, W. R.; Serin, J. M.; Edder, C.; Fréchet, J. M. J.; Matuszewski, M.; Tan, L. S.; Ohulchanskyy, T. Y.; Prasad, P. N. *J. Am. Chem. Soc.* **2004**, *126*, 5380−5381.
(8) Oar, M. A.; Serin, J. M.; Ditchel, W. R.; Fréchet, J. M. J.; Ohulchanskyy, T. Y.; Prasad, P. N. *Chem. Mater.* **2005**, *17*, 2267−2275.
(9) Belfield, K. D.; Bondar, M. V.; Yanez, C. O.; Hernandez, F. E.; Przhonska, O. V. *J. Phys. Chem. B* **2009**, *113*, 7101−7106.
(10) Belfield, K. D.; Bondar, M. V.; Morales, A. R.; Padilha, L. A.; Przhonska, O. V.; Wang, X. *ChemPhysChem* **2011**, *12*, 2755−2762.
(11) Wang, C.; Wang, X.; Shao, Z.; Zhao, X.; Zhou, G.; Wang, D.; Jiang, M. *Opt. Eng.* **2001**, *40*, 783−787.
(12) Wu, P. L.; Feng, X. J.; Tam, H. L.; Wong, M. S.; Cheah, K. W. *J. Am. Chem. Soc.* **2009**, *131*, 886−887.
(13) Buckup, T.; Weigel, A.; Hauer, J.; Motzkus, M. *Chem. Phys.* **2010**, *373*, 38−44.
(14) Changenet-Barret, P.; Espagne, A.; Katsonis, N.; Charier, S.; Baudin, J.-B.; Jullien, L.; Plaza, P.; Martin, M. M. *Chem. Phys. Lett.* **2002**, *365*, 285−291.
(15) Vorobyev, D. Y.; Kuo, C.-H.; Chen, J.-X.; Kuroda, D. G.; Scott, J. N.; Vanderkooi, J. M.; Hochstrasser, R. M. *J. Phys. Chem. B* **2009**, *113*, 15382−15391.
(16) Kosumi, D.; Kusumoto, T.; Fujii, R.; Sugisaki, M.; Iinuma, Y.; Oka, N.; Takaesu, Y.; Taira, T.; Iha, M.; Frank, H. A.; Hashimoto, H. *J. Lumin.* **2011**, *131*, 515−518.
(17) Fakis, M.; Polyzos, I.; Tsigaridas, G.; Giannetas, V.; Persephonis, P. *Chem. Phys. Lett.* **2004**, *394*, 372−376.
(18) Sajadi, M.; Dobryakov, A. L.; Garbin, E.; Ernsting, N. P.; Kovalenko, S. A. *Chem. Phys. Lett.* **2010**, *489*, 44−47.
(19) Maus, M.; Rettig, W.; Jonusauskas, G.; Lapouyade, R.; Rulliere, C. *J. Phys. Chem. A* **1998**, *102*, 7393−7405.
(20) Maciejewski, A.; Naskrecki, R.; Lorenc, M.; Ziolek, M.; Karolczak, J.; Kubicki, J.; Matysiak, M.; Szymanski, M. *J. Mol. Struct.* **2000**, *555*, 1−13.
(21) Li, F.-M.; Meng, F.-S.; Feng, W.-K.; Wang, S.-F.; Tian, H.; Gong, Q.-H. *Chin. Phys. Lett.* **2010**, *27*, 068202/1−4.
(22) Ramakrishna, G.; Goodson, T. *J. Phys. Chem. A* **2007**, *111*, 993−1000.
(23) Changenet, P.; Zhang, H.; van der Meer, M. J.; Glasbeek, M.; Plaza, P.; Martin, M. M. *J. Fluoresc.* **2000**, *10*, 155−160.
(24) Ishibashi, Y.; Fujiwara, M.; Umesato, T.; Saito, H.; Kobatake, S.; Irie, M.; Miyasaka, H. *J. Phys. Chem. C* **2011**, *115*, 4265−4272.
(25) Roland, T.; Ramirez, G. H.; Léonard, J.; Méry, S.; Haacke, S. *J. Phys., Conf. Ser.* **2011**, *276*, 1−6.
(26) Yang, S.; Liu, J.; Zhou, P.; Han, K.; He, G. *Chem. Phys. Lett.* **2011**, *512*, 66−69.
(27) Changenet-Barret, P.; Espagne, A.; Charier, S.; Baudin, J.-B.; Jullien, L.; Plaza, P.; Hellingwerf, K. J.; Martin, M. M. *Photochem. Photobiol. Sci.* **2004**, *3*, 823−829.
(28) Sheik-Bahae, M.; Said, A. A.; Wei, T. H.; Hagan, D. J.; Van Stryland, E. W. *IEEE J. Quantum Electron.* **1990**, *26*, 760−769.
(29) Xu, C.; Webb, W. W. *J. Opt. Soc. Am. B* **1996**, *13*, 481−491.
(30) Hell, S. W.; Wichmann, J. *Opt. Lett.* **1994**, *19*, 780−782.

(31) Betzig, E.; Patterson, G. H.; Sougrat, R.; Lindwasser, O. W.; Olenych, S.; Bonifacino, J. S.; Davidson, M. W.; Lippincott-Schwartz, J.; Hess, H. F. *Science* **2006**, *313*, 1642−1645.
(32) Won, Y.; Moon, S.; Yang, W.; Kim, D.; Han, W.-T.; Kim, D. Y. *Opt. Exp.* **2011**, *19*, 3396−3405.
(33) La Clair, J. J. *Angew. Chem.* **1998**, *37*, 325−329.
(34) Tang, H.-Z.; Fujiki, M.; Zhang, Z.-B.; Torimitsu, K.; Motonaga, M. *Chem. Commun.* **2001**, *23*, 2426−2427.
(35) Lakowicz, J. R. *Principles of Fluorescence Spectroscopy*; Kluwer: New York, 1999.
(36) Belfield, K. D.; Andrade, C. D.; Yanez, C. O.; Bondar, M. V.; Hernandez, F. E.; Przhonska, O. V. *J. Phys. Chem. B* **2010**, *114*, 14087−14095.
(37) Corredor, C. C.; Belfield, K. D.; Bondar, M. V.; Przhonska, O. V.; Yao, S. *J. Photochem. Photobiol. A: Photochem.* **2006**, *184*, 105−112.
(38) Lepkowicz, R. S.; Przhonska, O. V.; Hales, J. M.; Hagan, D. J.; Van Stryland, E. W.; Bondar, M. V.; Slominsky, Y. L.; Kachkovski, A. D. *Chem. Phys.* **2003**, *286*, 277−291.
(39) Miyasaka, H.; Murakami, M.; Okada, T.; Nagata, Y.; Itaya, A.; Kobatake, S.; Irie, M. *Chem. Phys. Lett.* **2003**, *371*, 40−48.
(40) Makarov, N. S.; Drobizhev, M.; Rebane, A. *Opt. Exp.* **2008**, *16*, 4029−4047.
(41) Rumi, M.; Ehrlich, J. E.; Heikal, A. A.; Perry, J. W.; Barlow, S.; Hu, Z. Y.; McCord-Maughon, D.; Parker, T. C.; Rockel, H.; Thayumanavan, S.; Marder, S. R.; Beljonne, D.; Bredas, J. L. *J. Am. Chem. Soc.* **2000**, *122*, 9500−9510.
(42) Belfield, K. D.; Bondar, M. V.; Kachkovsky, O. D.; Przhonska, O. V.; Yao, S. *J. Lumin.* **2007**, *126*, 14−20.
(43) Terenziani, F.; Painelli, A.; Katan, C.; Charlot, M.; Blanchard-Desce, M. *J. Am. Chem. Soc.* **2006**, *128*, 15742−15755.
(44) Horng, M. L.; Gardecki, J. A.; Papazyan, A.; Maroncelli, M. *J. Phys. Chem.* **1995**, *99*, 17311−17337.
(45) Belfield, K. D.; Bondar, M. V.; Yanez, C. O.; Hernandez, F. E.; Przhonska, O. V. *J. Mater. Chem.* **2009**, *19*, 7498−7502.
(46) Ohta, K.; Antonov, L.; Yamada, S.; Kamada, K. *J. Chem. Phys.* **2007**, *127*, 084504−1/12.
(47) Shafer, F. P. *Dye Lasers*; Springer-Verlag: New York, 1973.
(48) Losio, P. A.; Hunziker, C.; Günter, P. *Appl. Phys. Lett.* **2007**, *90*, 241103/3.
(49) Yoon, S. M.; Lee, J.; Je, J. H.; Choi, H. C.; Yoon, M. *ACS Nano* **2011**, *5*, 2923−2929.
(50) Kim, S.; Park, S. Y.; Yoshida, I.; Kawai, H.; Nagamura, T. *J. Phys. Chem. B* **2002**, *106*, 9291−9294.
(51) Yao, S.; Ahn, H. Y.; Wang, X. H.; Fu, J.; Van Stryland, E. W.; Hagan, D. J.; Belfield, K. D. *J. Org. Chem.* **2010**, *75*, 3965−3974.
(52) Andrade, C. D.; Yanez, C. O.; Qaddoura, M. A.; Wang, X.; Arnett, C. L.; Coombs, S. A.; Bassiouni, R.; Bondar, M. V.; Belfield, K. D. *J. Fluor.* **2011**, *21*, 1223−1230.